Springer

Dear Author

Here are the proofs of your article.

- You can submit your corrections **online,** via **e-mail** or by **fax**.
- For **online** submission please insert your corrections in the online correction form. Always indicate the line number to which the correction refers.
- You can also insert your corrections in the proof PDF and **email** the annotated PDF.
- For **fax** submission, please ensure that your corrections are clearly legible. Use a fine black pen and write the correction in the margin, not too close to the edge of the page.
- Remember to note the **journal title**, **article number**, and **your name** when sending your response via e-mail or fax.
- **Check** the metadata sheet to make sure that the header information, especially author names and the corresponding affiliations are correctly shown.
- **Check** the questions that may have arisen during copy editing and insert your answers/corrections.
- **Check** that the text is complete and that all figures, tables and their legends are included. Also check the accuracy of special characters, equations, and electronic supplementary material if applicable. If necessary refer to the *Edited manuscript*.
- The publication of inaccurate data such as dosages and units can have serious consequences. Please take particular care that all such details are correct.
- Please **do not** make changes that involve only matters of style. We have generally introduced forms that follow the journal's style.
- Substantial changes in content, e.g., new results, corrected values, title and authorship are not allowed without the approval of the responsible editor. In such a case, please contact the Editorial Office and return his/her consent together with the proof.
- If we do not receive your corrections **within 48 hours**, we will send you a reminder.
- Your article will be published **Online First** approximately one week after receipt of your corrected proofs. This is the **official first publication** citable with the DOI. **Further changes are, therefore, not possible.**
- The **printed version** will follow in a forthcoming issue.

Please note

After online publication, subscribers (personal/institutional) to this journal will have access to the complete article via the DOI using the URL:

`http://dx.doi.org/10.1007/s12237-011-9461-z`

If you would like to know when your article has been published online, take advantage of our free alert service. For registration and further information, go to: http://www.springerlink.com.

Due to the electronic nature of the procedure, the manuscript and the original figures will only be returned to you on special request. When you return your corrections, please inform us, if you would like to have these documents returned.

Metadata of the article that will be visualized in OnlineFirst

1	Article Title	**Salt Marsh Accretion and Storm Tide Variation: an Example from a Barrier Island in the North Sea**	
2	Article Sub- Title		
3	Article Copyright - Year	**Coastal and Estuarine Research Federation 2011 (This will be the copyright line in the final PDF)**	
4	Journal Name	Estuaries and Coasts	
5	Corresponding Author	Family Name	**Schuerch**
6		Particle	
7		Given Name	**Mark**
8		Suffix	
9		Organization	University of Kiel
10		Division	“The Future Ocean” Excellence Cluster, Institute of Geography
11		Address	Kiel , Germany
12		e-mail	schuerch@geographie.uni-kiel.de
13	Author	Family Name	**Rapaglia**
14		Particle	
15		Given Name	**J.**
16		Suffix	
17		Organization	University of Kiel
18		Division	“The Future Ocean” Excellence Cluster, Institute of Geography
19		Address	Kiel , Germany
20		e-mail	
21	Author	Family Name	**Liebetrau**
22		Particle	
23		Given Name	**V.**
24		Suffix	
25		Organization	IFM-GEOMAR
26		Division	“The Future Ocean” Excellence Cluster, Leibniz Institute of Marine Science
27		Address	Kiel , Germany
28		e-mail	

29		Family Name	**Vafeidis**
30		Particle	
31		Given Name	**A.**
32		Suffix	
33	Author	Organization	University of Kiel
34		Division	“The Future Ocean” Excellence Cluster, Institute of Geography
35		Address	Kiel , Germany
36		e-mail	
37		Family Name	**Reise**
38		Particle	
39		Given Name	**K.**
40		Suffix	
41	Author	Organization	Alfred Wegner Institute for Polar and Marine Research
42		Division	Waddenseastation Sylt
43		Address	Bremerhaven , Germany
44		e-mail	

45		Received	11 January 2011
46	Schedule	Revised	28 October 2011
47		Accepted	3 November 2011

48 Abstract

We reconstruct past accretion rates of a salt marsh on the island of Sylt, Germany, using measurements of the radioisotopes ^{210}Pb and ^{137}Cs, as well as historical aerial photographs. Results from three cores indicate accretion rates varying between 1 and 16 mm year^{-1}. Comparisons with tide gauge data show that high accretion rates during the 1980s and 1990s coincide with periods of increased storm activity. We identify a critical inundation height of 18 cm below which the strength of a storm seems to positively influence salt marsh accretion rates and above which the frequency of storms becomes the major factor. In addition to sea level rise, we conclude that in low marsh zones subject to higher inundation levels, mean storm strength is the major factor affecting marsh accretion, whereas in high marsh zones with lower inundation levels, it is storm frequency that impacts marsh accretion.

49 Keywords separated by ' - ' Salt marsh - Accretion rate - Geochronology - Storm activity - Barrier Island - Sylt

50 Foot note information

Estuaries and Coasts
DOI 10.1007/s12237-011-9461-z

Salt Marsh Accretion and Storm Tide Variation: an Example from a Barrier Island in the North Sea

Mark Schuerch · J. Rapaglia · V. Liebetrau · A. Vafeidis · K. Reise

Received: 11 January 2011 / Revised: 28 October 2011 / Accepted: 3 November 2011

Abstract We reconstruct past accretion rates of a salt marsh on the island of Sylt, Germany, using measurements of the radioisotopes ^{210}Pb and ^{137}Cs, as well as historical aerial photographs. Results from three cores indicate accretion rates varying between 1 and 16 mm year^{-1}. Comparisons with tide gauge data show that high accretion rates during the 1980s and 1990s coincide with periods of increased storm activity. We identify a critical inundation height of 18 cm below which the strength of a storm seems to positively influence salt marsh accretion rates and above which the frequency of storms becomes the major factor. In addition to sea level rise, we conclude that in low marsh zones subject to higher inundation levels, mean storm strength is the major factor affecting marsh accretion, whereas in high marsh zones with lower inundation levels, it is storm frequency that impacts marsh accretion.

Keywords Salt marsh · Accretion rate · Geochronology · Storm activity · Barrier Island · Sylt

M. Schuerch (✉) · J. Rapaglia · A. Vafeidis
"The Future Ocean" Excellence Cluster, Institute of Geography,
University of Kiel,
Kiel, Germany
e-mail: schuerch@geographie.uni-kiel.de

V. Liebetrau
"The Future Ocean" Excellence Cluster,
Leibniz Institute of Marine Science, IFM-GEOMAR,
Kiel, Germany

K. Reise
Waddenseastation Sylt,
Alfred Wegner Institute for Polar and Marine Research,
Bremerhaven, Germany

Introduction

Coastal salt marshes in the Wadden Sea (southeastern North Sea) are abundant leeward of the East Frisian and North Frisian barrier islands as well as in front of the dike system on the Dutch–German–Danish North Sea coast. Salt marshes serve as coastal protection structures by reducing the impact of waves on the upper shoreline (e.g., Möller 2006) and as important habitats for specialized plants and animals including migratory and breeding waterfowl and breeding birds (Reise et al. 2010). The existence of salt marshes is critically dependent on how fast sediment accretes relative to sea level rise (Orson et al. 1985; Redfield 1972).

Salt marshes are complex coastal features, governed by various physical and biological processes creating a system that exists in dynamic equilibrium with relative sea level rise (Allen 2000). Salt marsh accretion, defined as the vertical growth of the marsh, occurs when organic and/or inorganic sediments are deposited onto the marsh during inundation (allochthonous growth), as well as when salt marsh plants grow and decompose (autochthonous growth; Dijkema 1987; Kolker et al. 2009). Projected acceleration in SLR, however, may outpace accretion rates in the future, if an insufficient amount of material is deposited on the marsh surface (Kirwan and Temmerman 2009; Orson et al. 1985). Several investigators studied marsh response to mean sea level rise (French 1993; Kirwan and Temmerman 2009; e.g., Orson et al. 1985; Reed 1995); others investigated the influence of tidal range on salt marsh accretion (e.g., Chmura et al. 2001; Harrison and Bloom 1977; Kirwan and Guntenspergen 2010), but relatively little literature is available discussing the impact of non-tidal

short-term sea level variations on salt marsh accretion (Bartholdy et al. 2004; French 2006; Kolker et al. 2009; Temmerman et al. 2003b). While it is a widespread assumption that macrotidal environments are more resilient against SLR than microtidal environments (Kirwan and Guntenspergen 2010), Allen (2000) and Kolker et al. (2009) conclude that marsh accretion is dominated by wind-induced (short-term) sea level variations in microtidal and by SLR-induced long-term sea level variations in macrotidal environments. It remains unclear how wind-induced sea level variations enhance the resilience of the salt marsh and, in particular, whether many minor storms are more effective in triggering accretion than a few major storms. This is noteworthy as certain studies suggest that the storm activity in the German Bight has increased in recent years and will most likely increase in the near future leading to more frequent storm surges and/or higher storm surge water levels (Beniston et al. 2007; Fischer-Bruns et al. 2005; Rockel and Woth 2007; von Storch and Weisse 2008; Woth et al. 2006).

The goal of this work is to reconstruct the development of a back-barrier salt marsh on the island of Sylt, Germany, by using both ^{210}Pb and ^{137}Cs as geochronometers. ^{210}Pb and ^{137}Cs are often used for studying soil and sediment processes (Armentano and Woodwell 1975; Delaune et al. 1978; Goodbred and Kuehl 1998; He and Walling 1996b; Kolker et al. 2009). These data will be combined with information gathered from aerial photographs. We report how the marsh has been growing during the last decades and compare accretion rates with historical tide gauge data in order to infer how storm activity affects marsh accretion and its resilience against accelerated SLR.

Study Site

The island of Sylt is located in the German Wadden Sea (54°47′18″ N, 008°17′30″ E), in the southeastern North Sea (Fig. 1). Its core is made of Pleistocene protruding outcrops. About 7,000 years B.P., during a period of SLR deceleration (Milne et al. 2005), local sea level reached its current position and sandy spits were formed north and south of the original Pleistocene outcrop (Ahrendt and Thiede 2001). Sylt is an elongated barrier island with a total area of 99 km^2 extending 40 km from north to south and ranging from 1 to 13 km in width (Kelletat 1992). The western coastline is characterized by extensive beaches and dunes, and due to a relatively steep offshore elevation gradient, it is exposed to highly energetic wave activity from the North Sea (Ahrendt and Köster 1998). The sheltered eastern coastline is fringed by extensive tidal flats. Salt marshes are found in the transition zone from dunes to tidal flats and have a total area of approximately 5 km^2 (The Trilateral Monitoring and Assessment Program—TMAP 2006).

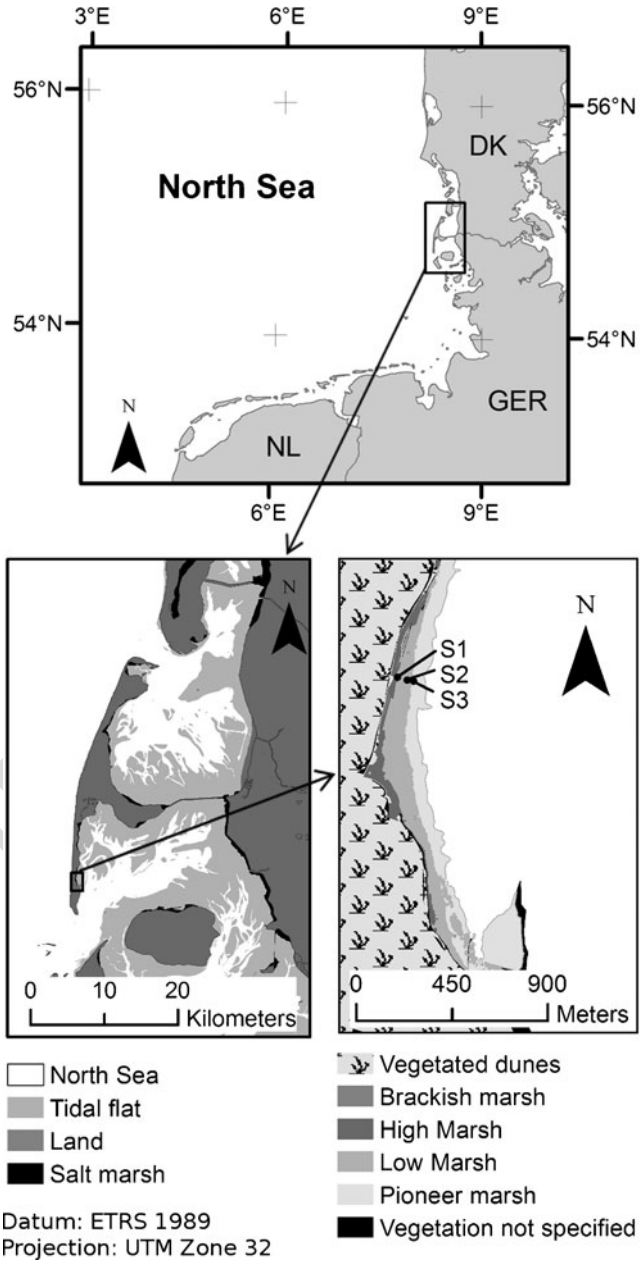

Fig. 1 The study area is located in the southeastern North Sea (*cell 1*), in the southern part of the island of Sylt (*cell 2*). The cores were taken on a transect in three dominant vegetation zones, indicated by points (*cell 3*)

The mean tidal range, as of 2010, at the nearby tide gauge *Hörnum Hafen* is 2.06 m (WSA—Wasser- und Schifffahrtsamt Tönning 2007), varying from 1.8 m at neap tide to 2.3 m at spring tide (BSH—Bundesamt für Seeschifffahrt und Hydrographie 2008). Tidal range has constantly increased in the Wadden Sea, including the *Hörnumtief*, since 1955 (Jensen and Mudersbach 2004).

The immediate study area is located in the southern third of Sylt between the villages of Rantum and Hörnum and is characterized by the typical morphology of a barrier island.

A transect from the open North Sea to the tidal flats is marked by a sequence of beaches, dunes, and salt marshes (Hildebrandt et al. 1993). These dunes developed a dense grass and scrub vegetation and became stable, as a consequence of intense planting activities since 1864 (ALW—Amt für Land- und Wasserwirtschaft Husum 1997). The area of the investigated marsh is about 0.3 km^2, with a length of about 2 km and a width ranging from 80 to 280 m. The salt marsh itself has a typical zonation ranging from pioneer marsh vegetation at the seaward edge to high marsh vegetation close to the foot of the dunes (Fig. 1). The pioneer marsh is dominated by the introduced cordgrass *Spartina anglica*, the low marsh zone is dominated by *Atriplex portulacoides*, and the high marsh zone is dominated by *Juncus gerardi* and *Elymus athericus*. The vegetation is not grazed by domestic livestock.

The elevation of the salt marsh ranges from about 0.7 to 1.5 m above NN (NN: German reference datum; Fig. 2), while the mean high water (MHW) level is at about 1 m (NN; WSA—Wasser- und Schifffahrtsamt Tönning 2007). The topography of the marsh is rather homogeneous, with a small marsh cliff (10–20 cm height) at the transition from pioneer to low marsh (Fig. 2). It is therefore assumed possible to reconstruct the historic evolution of this salt marsh by analyzing one transect only.

Methods and Analysis

Sample Collection and Preparation

Three marsh cores were collected on 22 January 2009 using PVC tubes with an inner diameter of 11.8 cm. Cores were collected on a shore-normal transect, within the three dominant vegetation zones (Figs. 1 and 2) and had a length of about 50–70 cm. S3, the most seaward core, was collected about 30 m from the seaward edge of the pioneer marsh, while S2 and S1 were located about 60 m and 110 m inland from the seaward edge, respectively (Fig. 2). The large diameter of the tube was chosen in order to reduce possible compaction of the soil during collection, as well as to amass a large volume of material for accurate analysis. Compaction during core collection was measured in situ as the difference between the measures from the top of the PVC tube to the salt marsh surface outside and inside the core. This difference was found to vary between 2% and 4% of the core length (in all three cores) and was therefore assumed to be negligible.

The transect where the cores were taken was leveled by hand using a dumpy level on a tripod. The height of the (seaward) starting point was determined by comparison of measured flooding and HW times between the starting point and the tide gauge in *Hörnum Hafen.* Elevations of the three core locations, as of today, are 0.94 m (S3), 1.34 m (S2), and 1.44 m (S1) above NN (Fig. 2). S3 is the only core location that is regularly inundated, while S1 and S2 are only inundated during storm tides.

After extraction, the cores were sliced into layers with a thickness of 1–5 cm. The thickness of the layers progressively increased toward the bottom of the core. The sediment was freeze-dried and ground manually in order to disintegrate the conglomerates of sediment. The ground material was filled into Petri dishes with a diameter of 52 mm and embedded into epoxy resin, which prevented ^{222}Rn from degassing. The dry weight of the aliquots embedded for radiometric analysis ranged from 17.25 to 43.44 g. Samples were allowed to sit for at least 3 weeks in order to reach equilibrium between ^{226}Ra and ^{214}Bi before analysis.

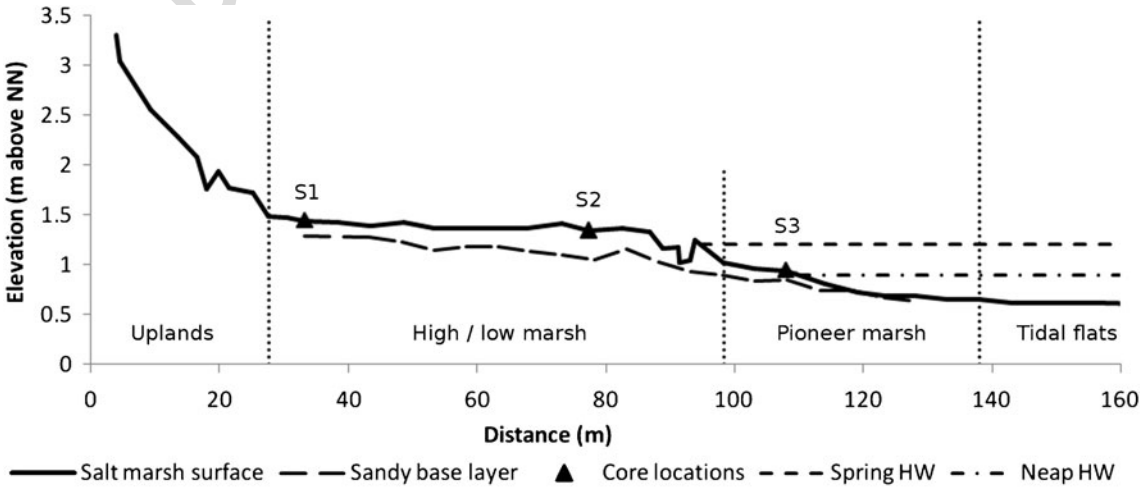

Fig. 2 Topographic profile and marsh zonation of the investigated salt marsh. Core locations and the sandy base layer are indicated by *triangles* and a *dashed line*, respectively

Sedimentology: Grain Size, Organic Carbon Content, and Bulk Density

Salt marsh sediment was analyzed for grain size, organic carbon content, and bulk density in order to derive the depths of the base layer and for calculation of radioisotope inventories. Grain size measurements were conducted using laser diffractometry (Malvern Instruments Ldt 2010). Although this method is supposed to measure grain sizes ranging from 0.02 to 2,000 μm (Malvern Instruments Ldt 2010), gradually increasing uncertainties in the coarser spectrum of grain sizes were observed during pre-measurements. Therefore, the sediment was sieved at 1,000 μm before the measurements. The preparation of the samples included the destruction of organic carbon, using H_2O_2, and iron if necessary, using sodium bicarbonate, sodium citrate, and sodium dithionite. The measurements were conducted at obscuration rates between 5% and 30%.

The organic carbon content was measured using the element analyzer Euro EA, which performs C/N analysis. The organic carbon is oxidized in the system and escapes as CO_2 into a gas chromatographer where total C (and N) content is determined.

The bulk density (ρ) was indirectly calculated from the organic carbon and the water content (O_C and W) in the samples as not enough sample material was available in the upper layers for direct measurement. Assuming a constant density for water (ρ_W=1.02 gcm^{-3}) and for mineral and organic matter (ρ_M=2.6 gcm^{-3}, ρ_O=1.2 gcm^{-3}, respectively), the bulk density was calculated using the following formula (Kolker et al. 2009):

$$\rho = \frac{1-W}{\frac{W}{\rho_W} + \frac{1-W}{(1-O_C \times \rho_M)+(O_C \times \rho_O)}} \quad (5)$$

Additional measurements on dry bulk density and relative water content were conducted on cores extracted on the 18 May 2011 in order to validate these bulk density calculations. It was shown that the results of the model fit the measured data (R^2=0.98, p<0.01).

Assessment of Autocompaction

Bulk density calculations were used for the assessment of autocompaction within the cores S1, S2, and S3. Bulk densities within the uppermost 5 cm of the salt marsh cores were investigated for autocompaction (Bartholdy et al. 2010), since variability of bulk density triggered by changes of grain size and organic carbon content in the lower parts of the core was too large to derive reliable estimates for autocompaction. A logarithmic curve (Eq. 6) was fitted through the calculated bulk density data (BDD) within the uppermost 5 cm.

$$\mathrm{BDD} = A \times 1\mathrm{n}(z) + B \quad (6)$$

where A and B are constants to be optimized and z is the depth of the respective salt marsh layer.

If the model was found to significantly represent the bulk density data (p<0.05), autocompaction was included into the calculation of accretion rates by decompacting the core. Decompaction was performed by calculating the thickness of a layer in depth z (T_z) to the time when it was deposited using the inverse version of the equation presented by Williams (2003):

$$T_z = \frac{\mathrm{BDD}_z}{\mathrm{BDD}_0} \times T_0 \quad (7)$$

where BDD_0 and T_0 are the bulk dry density and the thickness of today's surface layer, respectively.

Radiometric Measurements

^{137}Cs ($t_{1/2}$=30.2 years) is a product of nuclear fission and is highly particle reactive (He and Walling 1996b). In Europe, it is marked by two main periods of atmospheric fallout (1963 and 1986) producing two useful marker horizons (Delaune et al. 1978; Kirchner and Ehlers 1998; Pedersen et al. 2007). The ^{137}Cs peak around 1963 is produced by a series of tests of nuclear bombs during the 1950s and 1960s, while the 1986 peak is a result of the nuclear disaster in Chernobyl. Some authors have found an additional ^{137}Cs signal in cores taken along the North and the Baltic Sea, peaking between 1974 and 1977 (Andersen et al. 2000; Kunzendorf et al. 1998). However, given the low initial activity and the 30-year half-life of ^{137}Cs, these activities are probably below detection limits today. ^{210}Pb ($t_{1/2}$=22.3 years), on the other hand, is constantly being supplied from the atmosphere via the decay of its grandparent nuclide ^{222}Rn (Koide et al. 1972; Walling et al. 2003). This continuous deposition makes ^{210}Pb an excellent geochronometer for deriving accretion rates in coastal salt marshes (Appleby and Oldfield 1978, 1983; Bartholdy et al. 2004; Bellucci et al. 2007; Kirchner and Ehlers 1998).

A low-background coaxial Ge(Li)detector was employed to measure total gamma-ray activity of ^{210}Pb, ^{226}Ra, and ^{137}Cs. It is a non-destructive counting method that allows simultaneous measurement of all three radionuclides (Nikulina 2008). Measurement of ^{226}Ra is necessary because it is a proxy for supported ^{210}Pb. The analysis was conducted by the "Laboratory for Radioisotopes" in Goettingen, Germany. ^{210}Pb was measured via its gamma peak at 46.6 keV, ^{137}Cs via its peak at 661.7 keV, and ^{226}Ra via the peaks of its granddaughters ^{214}Pb and ^{214}Bi at 352

and 609.3/1,120.3 keV, respectively. The measurement time for all samples was 250,000 s.

Errors/Detection Limit

Errors generally increase toward the low energy gamma-ray spectrum, since the background radiation is elevated as a consequence of the Compton effect of higher energetic radionuclides (Compton 1923). Meanwhile, for higher energy spectra, the background radiation decreases continuously. For ^{210}Pb that is measured at 46.6 keV (very low energy), this is of particular importance, since the background radiation within the sample may be elevated above the ^{210}Pb activity of the soil sample, resulting in measurements below detection limit.

Another source of error for radiometric measurements is the background radiation of the environment, which is quantified by measuring a parallel blank sample and minimized by increasing the sample volume as well as the counting time. The combined "internal" and environmental background radiation at 46.6 keV is therefore higher than the activity measured for ^{226}Ra in higher energy spectra, and detection limits can be included into the analysis as maximum values for ^{210}Pb activities.

Dating Model

The constant rate of supply model (CRS) is employed for the dating of sediment characterized by variations of initial concentrations (Appleby and Oldfield 1978; Appleby and Oldfield 1983). It is therefore useful in study sites with irregular inundation, where accretion rates strongly vary with time. This model allows for the calculation of the age of the sediment by using radioisotope inventories (Appleby and Oldfield 1978; Kolker et al. 2009).

Due to the relative elevation of the core locations within the tidal frame (Fig. 2), irregular inundation occurs during storm surges, negating the assumption that accretion rates are constant over time. Therefore, the CRS model was used for this study.

Aerial Photographs

Aerial photographs of the investigated area, provided by the Landesbetrieb für Küstenschutz, Nationalpark und Meeresschutz Schleswig-Holstein (LKN-SH), were utilized in order to analyze the historic extension of the salt marsh during the last century and to verify the radiometric measurements. Photographs were available from 1937, 1958, 1988, 1999, 2003, and 2007. After georeferencing the pictures and overlaying the core locations, visual interpretation was performed in order to classify the core location into the categories "marsh" and "no marsh."

Hydrological Data

Annual data about mean sea level (MSL) were calculated from annual MHW and mean low water (MLW) levels (Hofstede 2010, personal communication). Storm frequency and storm intensity were aggregated from the high water levels, collected for every tidal cycle between 1938 and 2007 (Wahl 2010, personal communication; Wahl et al. 2011). Eustatic sea level rise was included into the analysis as an underlying trend that was removed from the original dataset before storm parameterization was conducted. Global SLR data, presented by Church and Church and White (2011), were used for that purpose due to a lack of reliable estimates of local eustatic SLR.

Storm activity was parameterized by storm frequency, defined as the number of tides above a certain storm level, and by storm intensity, defined as the mean height of these storm tides. For storm parameterization, we used these definitions in order to ensure that storm intensity is statistically independent from storm frequency. Mean sea level in turn was calculated as a function of MHW and MLW (Wahl et al. 2010).

Mean values of storm intensity and frequency data were aggregated for all years in which an estimate for accretion rate was available, using a moving average filter. Taking into account an expected error and temporal resolution of the dating of the sediment layers, the window size was chosen to be 5 years.

Analysis of Storm-Related Salt Marsh Accretion

One of the main objectives of this study is to investigate the influence of storm frequency and storm intensity on the observed accretion rates. Multiple linear regression analysis was employed to assess how much of the variation within the accretion rate time series can be explained by one of these parameters. This analysis was carried out by including all high water levels that flooded the marsh from 1938 to 2007. By gradually increasing the storm level and therefore excluding the low inundation events, we investigated how different high water levels were influencing accretion rates in the past. The standardized coefficients (β) of the multiple linear regressions, as well as the p values, were compared for the different storm levels.

Results

Grain Size Analysis and Organic Carbon Content, and Bulk Density

In each of the cores, a fine-grained upper layer is underlain by layers comprised of mainly coarse-grained

sediments. The transition zone in core S1 is very distinct, and fine-grained sediments are not present below a depth of about 10 cm (Fig. 3). In contrast, the transition zones in cores S2 and S3 are more gradual. Fine-grained sediment is, in fact, present throughout the entire core S2 (Fig. 3).

Bulk densities reproduce this pattern of fine-grained sediments on top of a coarse-grained base layer by increasing at the interfaces of salt marsh sediments and the sandy base layer (Fig. 3). In core S1, a clear increase of bulk density is observed at a depth of about 10 cm, reaching 1,574 kg m^{-3}. The high bulk density of 1,469 kg m^{-3} at the depth of 4.5 cm is considered as an outlier and was therefore excluded from the analysis. Instead, the average from the neighboring upper and lower layers was employed. The increase in S2 is more gradual and constant, with a maximum bulk density of 939 kg dm^{-3} at 27 cm. In core S3, a considerable increase in bulk density is observed at a depth of about 5 cm, with a maximum value of 1591 kg m^{-3}. Within the silty salt marsh sediments, bulk densities in cores S2 and S3 do not significantly increase, mostly varying between 500 and 600 kg m^{-3}. In core S1, a significant increase from 326 to 656 kg m^{-3} within the uppermost 6 cm is observed, and bulk density then decreases to 450–500 kg m^{-3} in the lower silty layers.

Salt marsh sediments are characterized by fine-grained material with high organic content, which allows for visual and experimental determination of the thickness of the marsh layer deposited on top of the sandy base. Herein, the base of the marsh can clearly be identified in cores S1 and S3 at 8.5 and 4.5 cm, respectively, whereas it is not as clear in core S2 (Fig. 3). The fine-grained fraction rapidly decreases at 21 cm but increases at 23 and 27 cm again. Although high fractions of sand at depths of 21 and 25 cm are found, marsh development seems to have started at a depth of about 27 cm.

The increase of bulk density within the uppermost 5 cm of core S1 was found to fit the logarithmic model (equation 6; R^2=0.97, p<0.02), which is considered as evidence for autocompaction. Model parameters A and B were estimated to be 0.0879 and 0.3791, respectively. The autocompaction rate during the growth of the salt marsh therefore averages 1 mm $year^{-1}$.

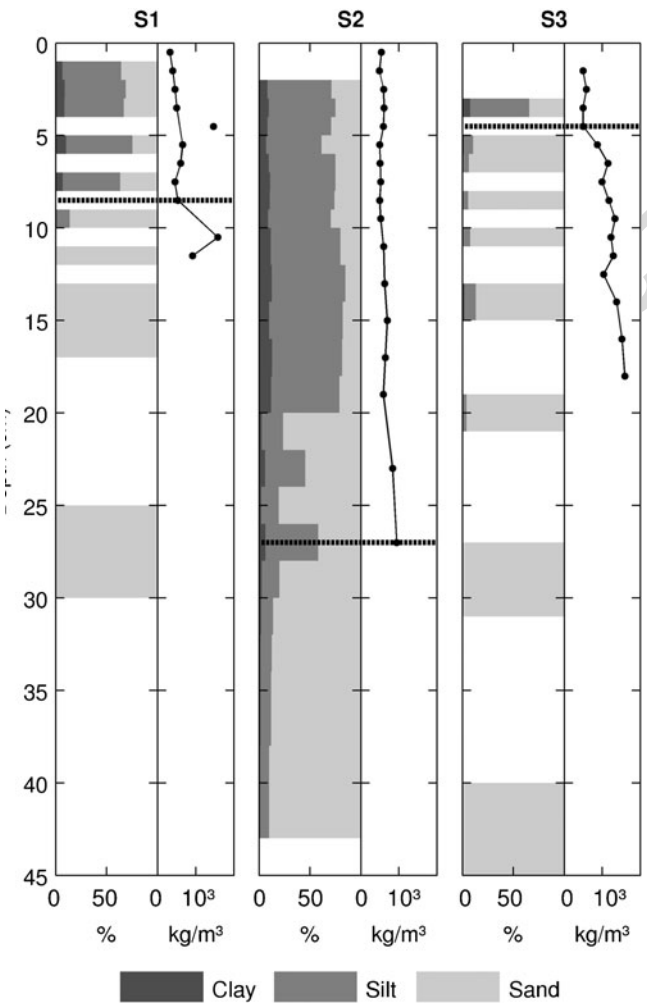

Q3 **Fig. 3** Grain size composition (in percent) and bulk density calculations (in kilograms per cubic meter), as described in Eq. 5, for all three cores and all depths (in centimeters) that were measured. Grain size composition is depicted in the *bar graph* and bulk density by the *line graph*. The depth of the sandy base layer is indicated by the *dashes line*

Aerial Photographs

The first photograph available, taken in 1937 (Fig. 4a), provides strong evidence for the presence of marsh at locations S1 and S2; however, no marsh is yet present at location S3. A sand bar seems to have formed between the seaward edge of the marsh and the adjacent tidal flat. At the landward edge of the marsh sand appears to be transported onto the marsh surface. However, in the following photograph from 1958 (Fig. 4b), sand transport onto the marsh at the landward edge seems to be less visible than in 1937; meanwhile, the sand bar at the seaward edge has developed further offshore. Recent photographs from 1988 and 1995 (Fig. 4c, d) do not show considerable changes of the marsh extension toward the land, but do indicate a seaward expansion. In 1988 (Fig. 4c), core location S3 is found to be in a channel between the developing pioneer marsh and the mature main part of the marsh. The photo from 1995 (Fig. 4d) shows that the channel appears to be closed and covered by pioneer marsh vegetation. Marsh development at core location S3 is, therefore, estimated to have started between 1988 and 1995.

JrnlID 12237_ArtID 9461_Proof# 1 - 23/11/2011

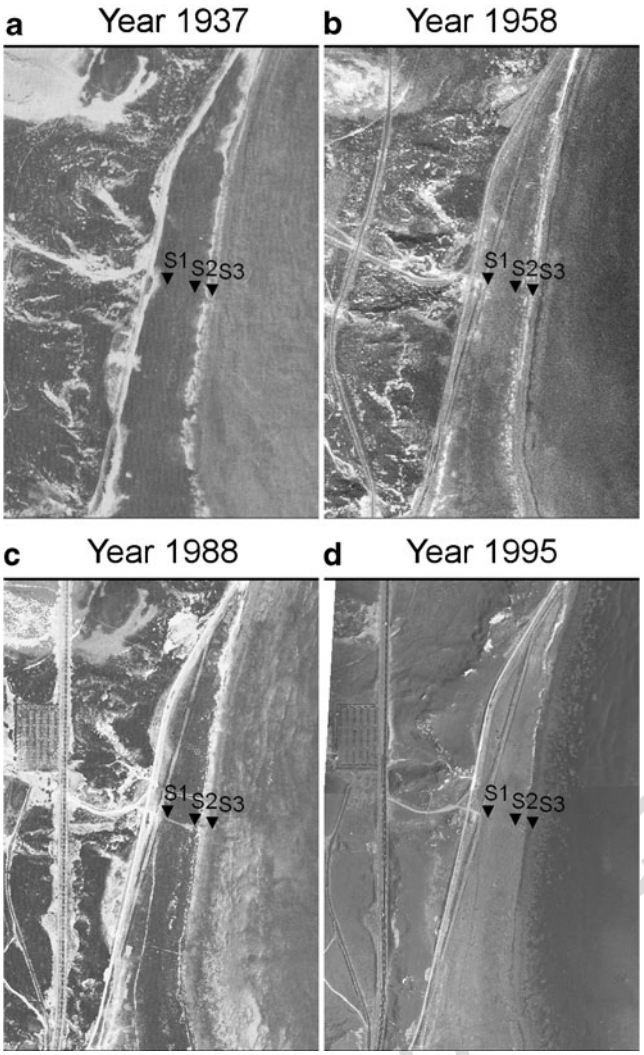

Fig 4 Aerial photographs of the investigated salt marsh from 1937 (**a**), 1958 (**b**), 1988 (**c**), and 1995 (**d**). *Dark colors* indicate vegetated areas. *Bright colors* indicate sand. Source: LKN-SH

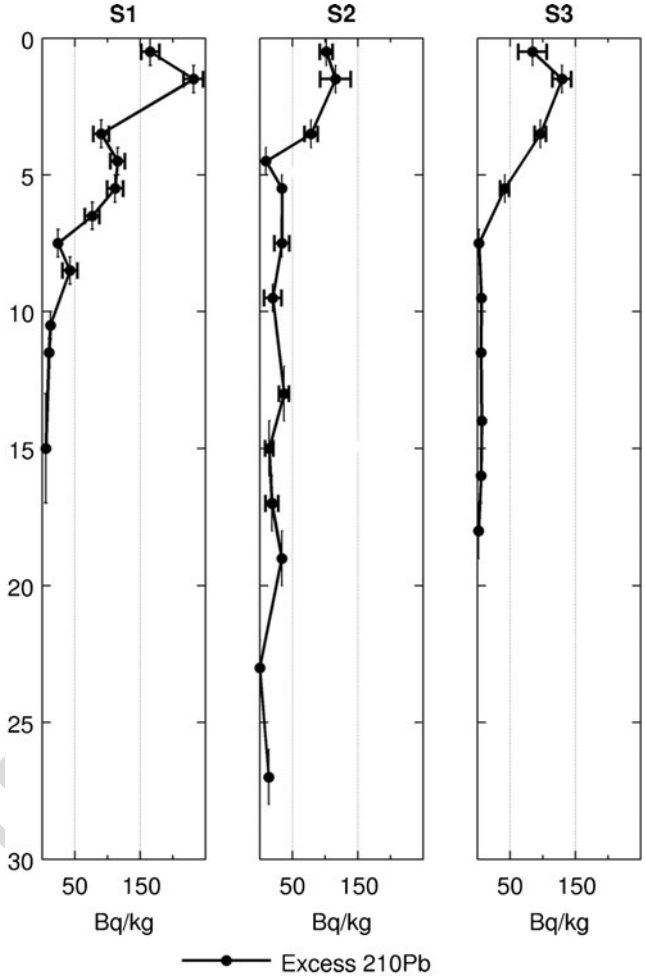

Fig. 5 Excess ^{210}Pb (in Becquerel per kilogram) in all three cores and all depths (in centimeters) that were measured. *Horizontal error bars* indicate propagated errors for excess ^{210}Pb. Measurements without *horizontal error bars* were measured below detection limit. *Vertical error bars* represent the thickness of the measured layer

Radioisotope Data

^{210}Pb Data

All three depth profiles of excess ^{210}Pb ($^{210}Pb_{XS}$) generally decrease as expected (Fig. 5). Large variations are found in the surface concentrations, with the highest activity (232 Bq kg^{-1} in 1.5 cm) in core S1. Distinct peaks are found at a depth of 1.5 cm in all three cores.

In core S1, a slow decrease is observed, due to relatively high activities (116, 112 Bq kg^{-1}) at depths of 4.5 and 5.5 cm. Activities below 10 cm are all less than the detection limit and therefore less than 12.6 Bq kg^{-1} (Fig. 5). The initial decrease in S2 is much greater and influenced by low activity at 4.5 cm (below detection limit of 9.5 Bq kg^{-1}). Activities below 4.5 cm decrease slower, eventually resulting in activities below the detection limit for all depths lower than 17 cm (Fig. 5). In core S3, $^{210}Pb_{XS}$ also quickly decreases within the upper 7 cm from 129 Bq kg^{-1} at 1.5 cm to less than 2.6 Bq kg^{-1} at 7.5 cm. $^{210}Pb_{XS}$ activities at lower depths are all below the detection limit (Fig. 5).

As ^{210}Pb activities in the sandy substrate of the cores S1 and S3 are all below the detection limit, normalization for grain size and organic carbon content of these activities is impossible. In core S2, where the fraction of fine-grained, highly organic sediment is rather constant within salt marsh layers, normalization is not necessary.

^{137}Cs Data

^{137}Cs peaks are found in cores S1 and S2. In core S3, no ^{137}Cs peak was found. S1 is characterized by a major peak at a depth of 5.5 cm (267 Bq kg^{-1}) and a minor peak at 8.5 cm (38 Bq kg^{-1}; Fig. 6). ^{137}Cs appears to decrease

toward zero at about 15 cm, although it should be considered that the sediment below 10 cm is very coarse and the effect of coarse-grained sediment might reduce the ^{137}Cs activity (He and Walling 1996a). In core S2, the situation is clearer: Two peaks are found in depths of 5.5 cm (64 Bq kg^{-1}) and 17 cm (52 Bq kg^{-1}); we note that the upper peak's activity is significantly lower than the activity in S1 (Fig. 6). The ^{137}Cs activity in core S3 is missing a distinct peak and has a very low activity (<1 Bq kg^{-1}) in the sandy base layer. Finer sediments in the upper layers are marked by a slight increase in activity up to 8 Bq kg^{-1} (Fig. 6).

Age of Base Layer

The age of the marsh and the mean accretion rates were determined by radioisotope dating (^{210}Pb) and compared with aerial photographs (Table 1). The base layer at core location S1 is found at a depth of about 8.5 cm (Figs. 2 and 3). Aerial photographs show that the marsh was present in 1937. However, analysis of ^{210}Pb data does not support this finding, suggesting the marsh to be younger. Several ^{210}Pb data in core S1 and S3 are below the detection limit due to a relatively high baseline activity in these samples. Since the detection limit is considered as a maximum activity and allows for activities within the range of zero to the detection limit, the original error range needs to be extended. Therefore, the year when the base layer was deposited (according to ^{210}Pb dating) is calculated to be between 1925 (±5 years) and 1955 (±5 years) (Table 1). Utilizing these dates and the aerial photographic evidence, we conclude that the marsh started to develop between 1925 (±5 years) and 1937, resulting in a mean accretion rate between 1 and 1.2 mm year^{-1}. In core S2, the base layer is found at a depth of 27 cm (Figs. 2 and 3). ^{210}Pb dating suggests that this layer was deposited in 1915 (±5 years). The aerial photograph of 1937 confirms the existence of the marsh at that time. Therefore, the mean accretion rate for core location S2 is estimated to be 2.8 mm year^{-1} (Table 1). S3 has a marsh layer that is only 4.5 cm thick (Figs. 2 and 3), but no ^{210}Pb measurement is available for the base layer at that depth. Meanwhile, the sample at 3.5 cm is calculated to be deposited in 1996, suggesting a mean accretion rate of 2.5 mm year^{-1}. Aerial photographs indicate the beginning of the pioneer (*Spartina*) marsh development between 1988 and 1995.

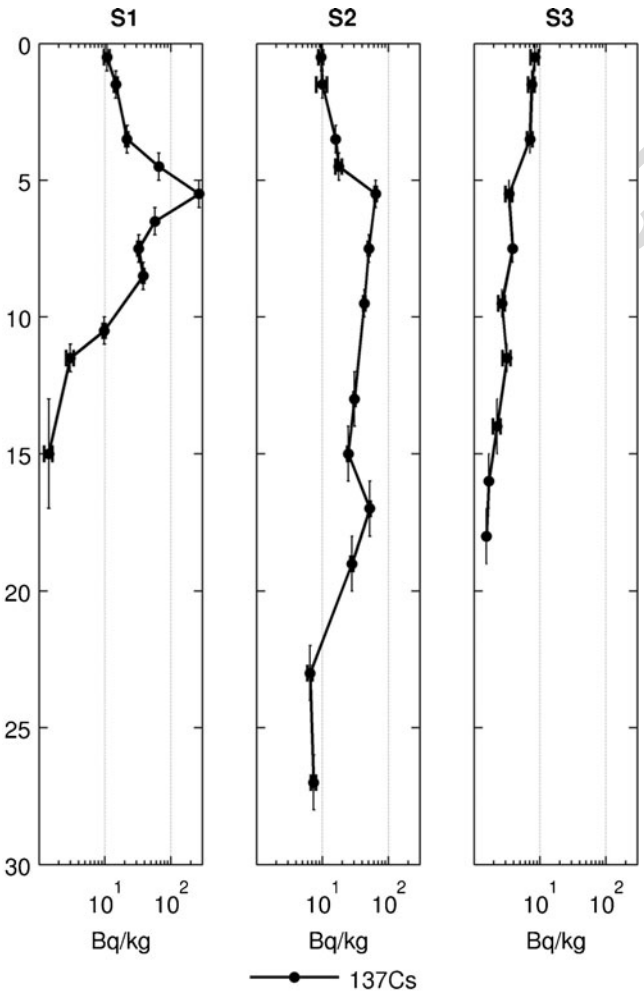

Fig. 6 ^{137}Cs (in Becquerel per kilogram) in all three cores and all depths (in centimeters) that were measured. *Horizontal error bars* indicate measurement errors of ^{137}Cs. *Vertical error bars* represent the thickness of the measured layer

Table 1 Ages of base layers and mean sedimentation rates: comparison of ^{210}Pb datings with information from aerial photographs

Core name	Depth of base layer	Age of base layer (^{210}Pb)	Age of base layer (aerial photographs)	Sedimentation rate (mm/year)
S1	8.5 cm	1925–1955	<1937	1–1.2
S2	27	1915	<1937	2.8
S3	4.5 cm	No measurement	1988–1995	2.5 (since 1996)

Accretion Rates

A reliable time series of accretion rates could only be drawn for the core S2 because the marsh layer in S3 is too thin to show significant variations, while ^{210}Pb dating for S1 resulted in small accretion rates associated with large uncertainties. However, for S1, a general trend toward an increase of accretion rates can be observed from the beginning of the 1960s, resulting in a recent accretion rate between 3 and 3.5 mm year^{-1}. Accretion rates for S2 indicate strong variations over the last 75 years, ranging from about 1 up to 16 mm year^{-1} (Fig. 7). No clear trend can be observed, although accretion rates in the 1980s and 1990s seem to be higher. Two distinct peaks are found in 1982 and 1992 (according to ^{210}Pb dating).

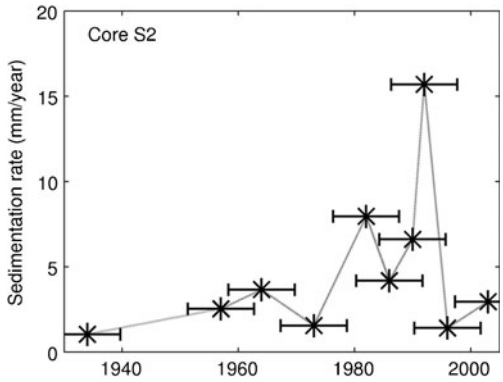

Fig. 7 Marsh sedimentation rates from 1938 to 2003 (millimeters per year). *Horizontal error bars* represent the averaged uncertainty of the ^{210}Pb dating

Hydrology and Meteorology

Tide gauge data from1938 to 2007 were analyzed for historic trends (Fig. 8) and compared to ^{210}Pb-derived marsh elevations (Fig. 9). It is shown that the MSL at the tide gauge *Hoernum Hafen* within that time period rose by about 2.1 mm year^{-1}, slightly greater than the global rate of SLR of 1.8 mm year^{-1} during the same period (Church and White 2011). The rise of MSL was accompanied by a mean increase of the MHW of about 4 mm year^{-1}, while the MLW did not change significantly. The increase of both MHW and MSL was observed to accelerate since about the early 1980s. This corresponds to data analyzed by Wahl et al. (2010), who further pointed out that SLR rates during the last 10–15 years within the German Bight were higher than the global average, as reported by Church et al. (2008).

The frequency of storm floods was analyzed based on their definition given by the German Maritime and Hydrographic Agency (BSH), where storm floods are water levels exceeding 1.5 m above MHW. Considering that the averaged yearly MHW from 1938 to 2007 is 0.9 m above NN, this corresponds to a storm level of 2.4 m NN. It was shown that storm frequency experienced a linear increase of 0.06 events year^{-1}, while 1984 and 1990 were marked by the greatest number of storms with 10 and 11 events, respectively. During the same period, the intensity of these storms did not significantly change.

As MHW increased rapidly within the last 50 years, salt marsh growth was not able to keep pace with this rise. An average of 2.6 and 1.3 mm year^{-1} was lost relative to MHW at core location S1 and S2, respectively. Core location S3 was observed to accrete at a rate of 2.5 mm year^{-1} since 1996. Meanwhile, during that period, MHW strongly increased with a rate of 11 mm year^{-1} (Fig. 9). Marsh elevation of S2 relative to MSL, on the other hand, increased by 0.7 mm year^{-1}, while S1 decreased by 0.6 mm year^{-1} (Fig. 9).

Influence of Storm Frequency and Intensity on Accretion Rates

The marsh at core location S2 floods when the water level reaches 134 cm (NN; Fig. 2). Multiple linear regression analysis shows that storm intensity (β=0.88, p<0.01) describes accretion rates better than storm frequency (β=0.06, p>0.1), when considering all inundation events (Fig. 10). However, with an increasing maximum storm

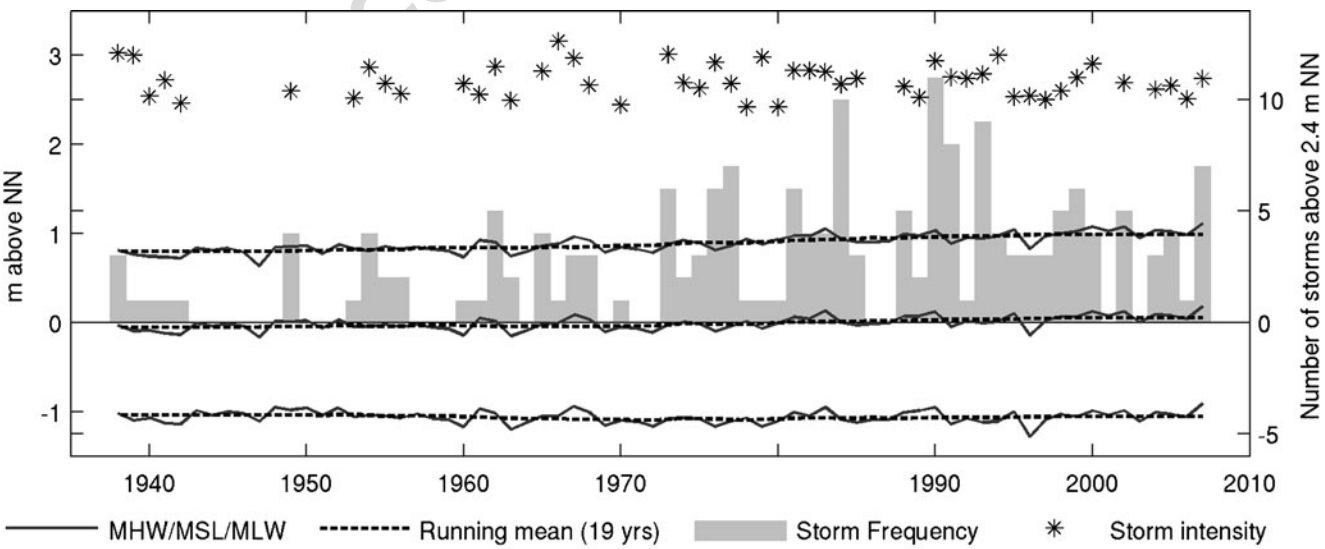

Fig. 8 Hydrological data from 1938 to 2007 at tide gauge *Hörnum Hafen* (Sylt). Storm intensity (*stars*), mean tidal high water (*MHW*), mean sea level (*MSL*), and mean tidal low water (*MLW*) are given in meter above "normal null" (*NN*). A 19-year running mean is given for MHW, MSL, and MLW. Storm frequency (*bars*) is the number of storm events that exceeded the level of 2.4 m above NN. Source: Wahl (2010, personal communication) and Hartwig (2010)

Q5/Q6

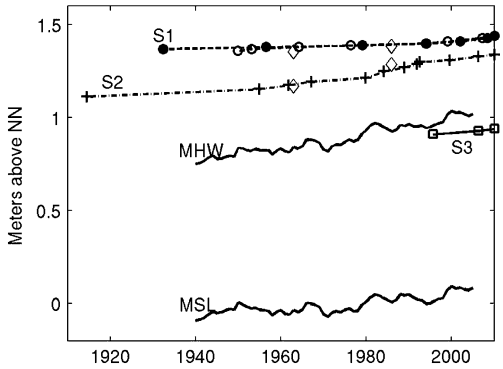

Fig. 9 Historic marsh elevations for all three cores derived from ^{210}Pb and ^{137}Cs data. Due to several data points below the detection limit in core S1, two graphs are displayed, comparing the fastest possible accretion rates (*open circles*) with the slowest possible accretion rates (*filled circles*). For validation of the data, the ^{137}Cs peaks are included (*open diamonds*). The error bars (as shown in Fig. 6) were omitted for clarity. The mean high water and the mean sea level (MHW and MSL: *solid lines*) are displayed as 5-year running averages

level, there is a decreasing influence of the storm intensity, whereas the influence of storm frequency gradually increases. At a storm level of 260 cm, for example, storm frequency gives a β of 0.86 ($p<0.01$), while storm intensity cannot explain accretion rates significantly ($\beta=0.04$, $p>0.1$; Fig. 11). It appears that the storm level of 152 cm (equals an inundation height of 18 cm at core location S2) is the turning point where the influence of storm frequency becomes statistically significant ($p<0.1$); meanwhile, the influence of storm intensity progressively diminishes (Fig. 12).

Discussion

^{210}Pb geochronologies were used at three salt marsh levels (a) to determine the age of the marsh and to reconstruct its evolution, (b) to assess temporal variations of accretion rates at all three core locations, and (c) to identify the hydrological parameters influencing marsh accretion.

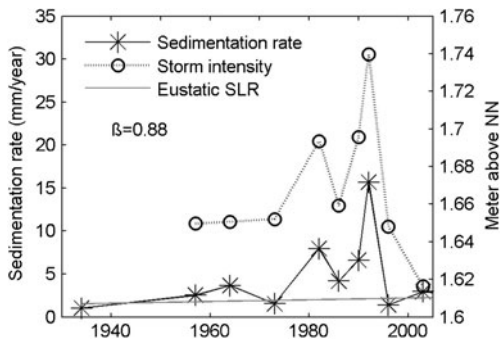

Fig. 10 Comparison of sedimentation rates (*stars*) at core location S2 with storm intensity (*open circles*), defined as the mean height for all high water levels exceeding 1.34 m (NN)

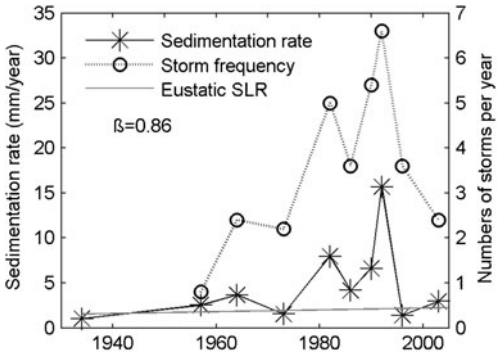

Fig. 11 Comparison of sedimentation rates (*stars*) at core location S2 with storm frequency (*open circles*), defined as the number of water levels, exceeding 2.4 m (NN)

Support for Accretion Rate Calculation

In contrast to the continuous deposition of ^{210}Pb on the marsh surface, ^{137}Cs serves as a marker horizon that can be used to calculate mean accretion rates in between the years 1963, 1986, and 2009, when the cores were extracted. It is, therefore, an additional independent geochronometer that allows for comparison with the ^{210}Pb dating method, but not for derivation of higher resolved temporal accretion rates. Both the 1963 and 1986 peaks were found in cores S1 and S2. In core S1, ^{137}Cs overestimates accretion rates compared to the ^{210}Pb data and the aerial photograph of 1937 (Fig. 9). It seems that ^{137}Cs has been transported further down in the soil column, although we are not certain of the mechanism. A very good agreement between the three methods (^{137}Cs, ^{210}Pb, and aerial photographs) is found in core S2 and in core S3. ^{137}Cs in core S2 shows

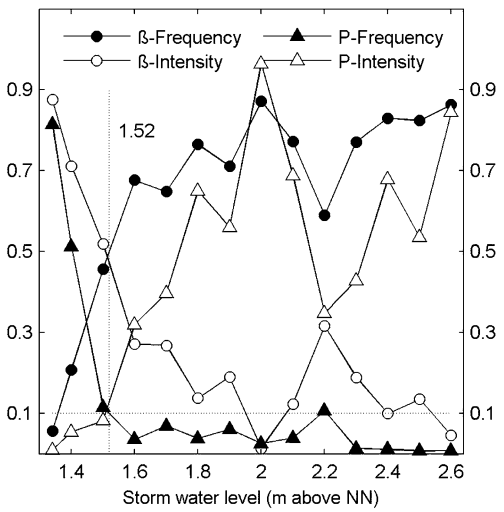

Fig. 12 Results of linear regression analysis: β and p values (*circles* and *triangles*, respectively) for different storm water levels (meters above NN) are shown. β and p values refer to results of multiple linear regression analyses of storm frequency (*filled symbols*) and storm intensity (*open symbols*) with sedimentation rates at core location S2

two distinct peaks at depths of 5.5 and 17 cm. ^{210}Pb dating is supported by these peaks; the layers at depths of 5.5 and 17 cm were estimated to be deposited in 1992 and 1961, respectively (Fig. 9). The absence of a peak in core S3 also supports what we can observe in the aerial photographs, as well as the ^{210}Pb dating suggesting that the marsh development started after 1988.

Grain size data also support the ^{210}Pb dating in core S2 to a certain degree. Two layers (5.5 and 9.5 cm) show an elevated fraction of coarse-grained sediments in comparison to the other layers (Fig. 3). ^{210}Pb dating calculates that these layers were deposited in 1992 (±5 years) and 1985 (±5 years). In 1990, the highest number of storms occurred during the last 70 years (Fig. 8), two of which were among the five most severe storm surges (measured at *Hörnum Hafen*) in recorded history. Meanwhile, the year 1984 was marked by the second most frequent storm events during the last 70 years (Fig. 8). We expect that the higher energy of storms allows for the transport of coarser-grained materials onto the marsh by both waves and currents.

Mean Accretion Rates

The spatial pattern of mean accretion rates shows a decrease from the low marsh toward the inner marsh (Table 1). This is a typical spatial phenomenon observed on many marshes by various authors (Bartholdy et al. 2004; Cahoon and Reed 1995; French and Spencer 1993; Pethick 1981; Temmerman et al. 2003a). Meanwhile, the mean accretion rate for the pioneer marsh zone is lower than the one in the low marsh zone. Resuspension of sediment during the early stage of the marsh development could be the reason for this pattern. The measured accretion rates generally compare well with mean accretion rates measured on the peninsula of Skallingen, where Bartholdy et al. (2004) found the accretion rate on the Skallingen marsh to vary between 2 mm year^{-1} on the inner marsh and 4 mm year^{-1} on the outer marsh. Measurements of Kirchner and Ehlers (1998) in the eastern part of Sylt, however, have shown much higher accretion rates between 5.8 and 15.2 mm year^{-1}, but grain sizes in this section of Sylt are much finer, indicating different hydrodynamic conditions favoring settling of sediment.

Temporal Variations of Accretion Rates

S2 shows strong temporal variations of accretion with a period of higher rates found during the 1980s and 1990s including two distinct peaks in 1982 and 1992 and a rapid decrease in accretion rates during the last 20 years. This pattern strongly resembles the periods of high storm activity (Figs. 10 and 11). Although temporal variations of accretion rates in S1 should only be considered as an approximation, a trend toward increasing accretion rates to current values between 3 and 3.5 mm year^{-1} is observed. The few data points that exist for S3 show a constant accretion rate of 2.5 mm year^{-1}.

Accretion rates at core location S2 during calm periods seem to lie close to the rates of eustatic SLR (Figs. 10 and 11), while, during stormy years, accretion rates are much higher than SLR. This behavior shows the importance of storms for the resilience of salt marshes toward eustatic SLR. Even though accretion rates during calm years are still sufficiently high, a considerable decrease in storminess would lower the marsh elevation and possibly affect the marsh zonation.

Historic Development of the Marsh

Using the data presented in the previous section, it is possible to reconstruct the historic evolution of the marsh: Marsh development at our study site seems to have started after about 1915. Prior to marsh development, we assume a bare sandy beach slope at that location. The age of the base layer at core location S2 indicates that marsh development started during a period of rapidly increasing MHW and MLW levels (Jensen and Mudersbach 2004; Wahl et al. 2010). Increasing inundation frequencies may have triggered the development of pioneer marsh vegetation, such as *Salicornia* and *Suaeda*, probably sheltered by a seaward sandy ridge. At some point, the sandy ridge at the seaward edge moved offshore and a cliff arose due to increased hydrodynamics caused by more frequent inundation events. As a consequence, a channel developed in front of the marsh, which probably acted as a tidal channel, building up levees at the landward and seaward side (Pedersen and Bartholdy 2007). According to the aerial photograph in 1988, the pioneer marsh started to develop on top of the sand bar and slowly spread toward the cliff at the marsh edge, stabilizing the latter. Decreased hydrodynamics in the vicinity of the sand bar, a constantly low MLW level, and a spread of the invasive species *S. anglica* after 1987 (Loebl et al. 2006) may have triggered that process. Today the cliff is located far inside the marsh, and the pioneer marsh seems to expand further onto the tidal flat and accrete faster than MSLR.

The inner part of the marsh accreted with the slowest overall accretion rate. While the base layer is approximately 30 cm above the base layer in the central part of the marsh, marsh development started between 1925 and 1937. During the first few decades of growth, aerial photographs indicate that considerable amounts of sand may have been blown onto this part of the marsh, although accretion rates were too low to detect significant temporal variations. The topography of the marsh platform has been flattened during the last 75 years due to higher accretion rates in the middle of the marsh than on the landward side of the marsh.

Influence of Storms on Accretion

The analysis presented in this study focuses on the historical vertical development of a single salt marsh. It is shown that an increase of storminess positively correlates with marsh accretion rates. While many authors have focused on the destructive, erosional influence of storms on salt marshes (e.g., Callaghan et al. 2010; Mariotti and Fagherazzi 2010; van de Koppel et al. 2005), our methods are not able to reproduce the lateral marsh development and their implications on accretion processes but rather the vertical marsh accretion.

Vertical accretion (at core location S2) was shown to be closely linked to past storm patterns with accretion rates of up to 16 mm year^{-1} in very stormy years. Linear regression analysis showed that both storm intensity and storm frequency are important factors influencing accretion rates. Storm frequency does not seem to be the driving factor of accretion if storm levels do not rise higher than 18 cm above the marsh surface at S2. The importance of frequency greatly increases above this threshold level (Fig. 12). We hypothesize that the presence and the height of the vegetation could be the reason for this threshold.

Assuming that the threshold value we found for the core S2 is true for different marsh elevations as well, we can identify two different driving factors for marsh accretion in the lower and the higher parts of the marsh: In the lower marsh zones, where inundation is frequent and usually higher than the vegetation height, accretion rates increase with increasing inundation frequency. Inundation frequency at low elevations, in turn, is highly correlated with the MHW level and possibly caused by SLR. In the higher parts of the marsh, where inundation is less frequent and heights of the inundation are often lower or just slightly higher than the vegetation height, we expect the mean strength of the storms to be more important than the actual number of storms.

These findings are especially relevant when considering possible implications on storm-related accretion processes. Assuming that more sediment is in suspension when storm water levels are high, the solution of the mass balance equation for incoming and settling sediment (Mudd et al. 2010; Temmerman et al. 2003a) results in an exponential increase of accretion rates with higher storm water levels (Fig. 13; Temmerman et al. 2003a). Considering our results, the effect of storm intensity on salt marsh accretion is suggested to be stronger at low storm water levels than at high storm water levels, resulting in a logarithmic rather than an exponential relationship between storm water levels and accretion rates (Fig. 13). The height at which the logarithmic curve starts to flatten is hypothesized to be connected to the height of the vegetation. Vegetation has a strong effect on flow velocities and the Reynolds number

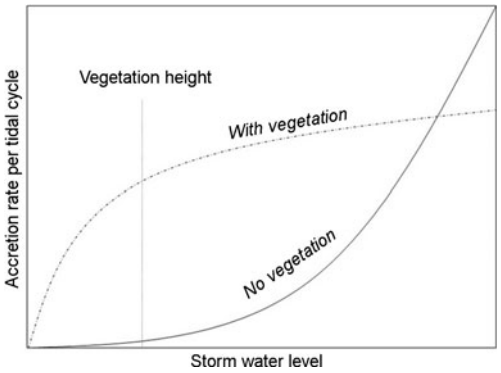

Fig. 13 Conceptual scheme of how vegetation is influencing accretion rates at various storm water levels. The "no vegetation scenario" does not reflect the resuspension happening in absence of a vegetation canopy

within the vegetation canopy and can therefore influence the flocculation and break-up processes of the sediment in suspension (Winterwerp 2002). Low flow velocities within the vegetation canopy could therefore result in larger floc sizes and corresponding settling velocities, while high flow velocities could decrease the floc sizes and decrease the settling velocities of the sediment particles (Bartholomä et al. 2009). This would infer that the depth-averaged settling velocity would decrease with inundation heights that exceed the vegetation height and result in a flatting of the above mentioned curve. We must emphasize that this hypothesis should be further investigated by explicitly examining flocculation processes over salt marsh surfaces during storm events.

Conclusions

In accordance with the available literature, ^{210}Pb has proven to be a good tool for determination of sediment accretion rates on salt marshes. ^{137}Cs data and aerial photographs independently supported the ^{210}Pb dating and the derived accretion rates. However, restrictions and limitation of the method can be recognized in core S1 and S3. Based on the results of this study, we make the following conclusions:

1. While not always coincident with one another, both storm frequency and intensity seem to affect salt marsh accretion rates. In very stormy years, accretion rates can increase 5-fold above mean value. Frequent and strong storms have shown that they can lead to accretion rates which are higher than MSLR and therefore are considered as an important factor for the ability of marshes to keep pace with eustatic SLR.
2. We show that eustatic SLR slightly increases accretion rates during calm wind periods, while a surplus of accretion is observed in stormy years, leading to a net increase of marsh elevation relative to mean sea level,

accompanied by a slight decrease in elevation relative to the more rapidly rising mean tidal high water level.

3. There exists a threshold for inundation depth (18 cm) on the investigated marsh at which the relative importance of storm frequency and intensity reverses. Storm intensity seems to be the driving factor for high accretion rates below an inundation depth of 18 cm, while storm frequency is more important above this inundation depth. The influence of vegetation is suggested to be the reason for this threshold.
4. The existence of a threshold for inundation depth implies that accretion of higher marsh zones is crucially dependent on the storm intensity, while lower marsh parts rather depend on the development of storm frequency and mean high water level, possibly influenced by a mean sea level rise. The different major driving factors for the marsh zones may lead to changes in marsh zonation, if storm activity and SLR rate change in the future.

Further investigation, including short-term measurements of accretion rates during storm events and modeling, is necessary to better understand the singular effects of storm intensity, storm frequency, and sea level rise on accretion processes. Also, more marshes in mesotidal environments need to be investigated to test whether a similar critical inundation depth threshold exists elsewhere and the hypothesis of vegetation being responsible can be verified.

Acknowledgments This project was funded by the Cluster of Excellence 80 "The Future Ocean." The "Future Ocean" is funded within the framework of the Excellence Initiative by the Deutsche Forschungsgemeinschaft on behalf of the German federal and state governments. Furthermore, we would like to thank Anton Eisenhauer for his support and the "Laboratory for Radioisotopes" in Goettingen for running the radiometric measurements. For their help in the field and during the preparation of the samples, we thank Daniela Arp, Michal Lichter, Tina Geissler, Natalia Zamora, and Claudia Wolff. The hydrological data for the tide gauge *Hörnum Hafen* were kindly supplied by Thomas Wahl, Jacobus Hofstede, and Gerd Hartwig. We would also like to thank the two anonymous reviewers for their valuable comments, which have helped in improving this manuscript.

References

Ahrendt, K. and R. Köster. 1998. Sylt—einst und jetzt. In *Umweltatlas Wattenmeers, Band 1*, Nordfriesisches und Dithmarscher Wattenmeer, eds. Nationalpark Schleswig-Holsteinisches Wattenmeer (Tönning) and Umweltbundesamt (Berlin), 38–39. Stuttgart: Eugen Ulmer.

Ahrendt, K., and J. Thiede. 2001. Naturräumliche Entwicklung Sylts—Vergangenheit und Zukunft. In *Sylt—Klimafolgen für Mensch und Küste*, ed. A. Daschkeit and P. Schottes, 69–112. Berlin: Springer.

Allen, J.R.L. 2000. Morphodynamics of Holocene salt marshes: A review sketch from the Atlantic and Southern North Sea coasts of Europe. *Quaternary Science Reviews* 19: 1155–1231.

ALW—Amt für Land- und Wasserwirtschaft Husum. 1997. *Fachplan Küstenschutz Sylt—Fortschreibung*. Husum: ALW.

Andersen, T.J., O.A. Mikkelsen, A.L. Møller, and P. Morten. 2000. Deposition and mixing depths on some European intertidal mudflats based on 210Pb and 137Cs activities. *Continental Shelf Research* 20: 1569–1591.

Appleby, P.G., and F. Oldfield. 1978. The calculation of lead-210 dates assuming a constant rate of supply of unsupported 210Pb to the sediment. *Catena* 5: 1–8.

Appleby, P.G., and F. Oldfield. 1983. The assessment of 210Pb data from sites with varying sediment accumulation rates. *Hydrobiologia* 103: 29–35.

Armentano, T.V., and G.M. Woodwell. 1975. Sedimentation rates in a Long Island marsh determined by 210 Pb dating. *American Society of Limnology and Oceanography* 20: 452–456.

Bartholdy, J., C. Christiansen, and H. Kunzendorf. 2004. Long term variations in backbarrier salt marsh deposition on the Skallingen peninsula—the Danish Wadden Sea. *Marine Geology* 203: 1–21.

Bartholdy, J., J.B.T. Pedersen, and A.T. Bartholdy. 2010. Autocompaction of shallow silty salt marsh clay. *Sedimentary Geology* 223: 310–319.

Bartholomä, A., A. Kubicki, T. Badewien, and B. Flemming. 2009. Suspended sediment transport in the German Wadden Sea—seasonal variations and extreme events. *Ocean Dynamics* 59: 213–225.

Bellucci, L.G., M. Frignani, J.K. Cochran, S. Albertazzi, L. Zaggia, G. Cecconi, and H. Hopkins. 2007. Pb-210 and Cs-137 as chronometers for salt marsh accretion in the Venice Lagoon—links to flooding frequency and climate change. *Journal of Environmental Radioactivity* 97: 85–102.

Beniston, M., D. Stephenson, O. Christensen, C. Ferro, C. Frei, S. Goyette, K. Halsnaes, T. Holt, K. Jylhä, B. Koffi, J. Palutikof, R. Schöll, T. Semmler, and K. Woth. 2007. Future extreme events in European climate: An exploration of regional climate model projections. *Climatic Change* 81: 71–95.

BSH—Bundesamt für Seeschifffahrt und Hydrographie. 2008. *Gezeitentafeln 2009—Europäische Gewässer*. Hamburg: BSH.

Cahoon, D.R., and D.J. Reed. 1995. Relationships among marsh surface topography, hydroperiod, and soil accretion in a deteriorating Louisiana salt marsh. *Journal of Coastal Research* 11: 357–369.

Callaghan, D.P., T.J. Bouma, P. Klaassen, D. Van der Wal, M.J.F. Stive, and P.M.J. Herman. 2010. Hydrodynamic forcing on salt-marsh development: Distinguishing the relative importance of waves and tidal flows. *Estuarine, Coastal and Shelf Science* 89: 73–88.

Chmura, G.L., A. Coffey, and R. Crago. 2001. Variation in surface sediment deposition on salt marshes in the Bay of Fundy. *Journal of Coastal Research* 17: 221–227.

Church, J., and N. White. 2011. Sea-level rise from the late 19th to the early 21st century. *Surveys in Geophysics* 32: 585–602.

Church, J., N. White, T. Aarup, W. Wilson, P. Woodworth, C. Domingues, J. Hunter, and K. Lambeck. 2008. Understanding global sea levels: Past, present and future. *Sustainability Science* 3: 9–22.

Compton, A.H. 1923. A quantum theory of the scattering of X-rays by light elements. *Physical Review* 21: 483–502.

De Groot, A. 2009. Salt-marsh sediment: Natural γ-radioactivity and spatial patterns. Ph.D. thesis, University of Groningen, Groningen. Q7

Delaune, R.D., W.H. Patrick, and R.J. Buresh. 1978. Sedimentation rates determined by 137Cs dating in a rapidly accreting salt marsh. *Nature* 275: 532–533.

Dijkema, K.S. 1987. Geography of salt marshes in Europe. *Zeitschrift Fur Geomorphologie* 31: 489–499.

Fischer-Bruns, I., H. Storch, J. González-Rouco, and E. Zorita. 2005. Modelling the variability of midlatitude storm activity on decadal to century time scales. *Climate Dynamics* 25: 461–476.

French, J.R. 1993. Numerical simulation of vertical marsh growth and adjustment to accelerated sea-level rise, North Norfolk, U.K. *Earth Surface Processes and Landforms* 18: 63–81.

French, J. 2006. Tidal marsh sedimentation and resilience to environmental change: Exploratory modelling of tidal, sea-level and sediment supply forcing in predominantly allochthonous systems. *Marine Geology* 235: 119–136.

French, J.R., and T. Spencer. 1993. Dynamics of sedimentation in a tide-dominated backbarrier salt marsh, Norfolk, UK. *Marine Geology* 110: 315–331.

Goodbred, S.L., and S.A. Kuehl. 1998. Floodplain processes in the Bengal Basin and the storage of Ganges-Brahmaputra river sediment: An accretion study using 137Cs and 210Pb geochronology. *Sedimentary Geology* 121: 239–258.

Harrison, E.Z., and A.L. Bloom. 1977. Sedimentation rates on tidal salt marshes in Connecticut. *Journal of Sedimentary Research* 47: 1484–1490.

He, Q., and D.E. Walling. 1996a. Interpreting particle size effects in the adsorption of 137Cs and unsupported 210Pb by mineral soils and sediments. *Journal of Environmental Radioactivity* 30: 117–137.

He, Q., and D.E. Walling. 1996b. Use of fallout Pb-210 measurements to investigate longer-term rates and pattern of overbank sediment deposition on the floodplains of lowland rivers. *Earth Surface Processes and Landforms* 21: 141–154.

Hildebrandt, V., J. Gemperlein, U. Zeltner, and W. Peteresen. 1993. *Landesweite Biotopkartierung—Kreis Nordfriesland: Landschaftsentwicklung—Aktuelle Situation—Flächenschutz*. Kiel: Landesamt für Naturschutz und Landschaftspflege Schleswig-Holstein.

Jensen, J., and C. Mudersbach. 2004. Zeitliche Änderungen in den Wasserstandszeitreihen an den Deutschen Küsten. In *Klimaänderung und Küstenschutz, Conference proceedings*, ed. G. Gönnert, H. Grassl, D. Kelletat, H. Kunz, B. Probst, H. von Storch, and J. Sündermann, 115–128. Hamburg: Universität Hamburg.

Kelletat, D. 1992. Coastal erosion and protection measures at the German North Sea Coast. *Journal of Coastal Research* 8: 699–711.

Kirchner, G., and H. Ehlers. 1998. Sediment geochronology in changing coastal environments: Potentials and limitations of the 137Cs and 210Pb methods. *Journal of Coastal Research* 14: 483–492.

Kirwan, M.L., and G.R. Guntenspergen. 2010. Influence of tidal range on the stability of coastal marshland. *Geophysical Research Letters* 115: F02009.

Kirwan, M., and S. Temmerman. 2009. Coastal marsh response to historical and future sea-level acceleration. *Quaternary Science Reviews* 28: 1801–1808.

Kirwan, M.L., G.R. Guntenspergen, A. D'Alpaos, J.T. Morris, S.M. Mudd, and S. Temmerman. 2010. Limits on the adaptability of coastal marshes to rising sea level. *Geophysical Research Letters* 37: L23401.

Koide, M., A. Soutar, and E.D. Goldberg. 1972. Marine geochronology with 210Pb. *Earth and Planetary Science Letters* 14: 442–446.

Kolker, A.S., S.L. Goodbred Jr., S. Hameed, and J.K. Cochran. 2009. High-resolution records of the response of coastal wetland systems to long-term and short-term sea-level variability. *Estuarine, Coastal and Shelf Science* 84: 493–508.

Kunzendorf, H., K.-C. Emeis, and C. Christiansen. 1998. Sedimentation in the Central Baltic Sea as viewed by non-destructive Pb-210-dating. *Geografisk Tidsskrift* 98: 1–8.

Loebl, M., J. Beusekom, and K. Reise. 2006. Is spread of the neophyte *Spartina anglica* recently enhanced by increasing temperatures? *Aquatic Ecology* 40: 315–324.

Malvern Instruments Ldt. 2010. Mastersizer 2000. http://www.malvern.de/LabGer/products/Mastersizer/MS2000/mastersizer2000.htm. Accessed 31 Aug 2010.

Mariotti, G.A., and S. Fagherazzi. 2010. A numerical model for the coupled long-term evolution of salt marshes and tidal flats. *Journal of Geophysical Research* 115: F01004.

Milne, G.A., A.J. Long, and S.E. Bassett. 2005. Modelling Holocene relative sea-level observations from the Caribbean and South America. *Quaternary Science Reviews* 24: 1183–1202.

Möller, I. 2006. Quantifying saltmarsh vegetation and its effect on wave height dissipation: Results from a UK East coast saltmarsh. *Estuarine, Coastal and Shelf Science* 69: 337–351.

Mudd, S.M., A. D'Alpaos, and J.T. Morris. 2010. How does vegetation affect sedimentation on tidal marshes? Investigating particle capture and hydrodynamic controls on biologically mediated sedimentation. *Journal of Geophysical Research* 115: F03029.

Nikulina, A. 2008. The imprint of anthropogenic activity versus natural variability in the fjords of Kiel Bight: Evidence from sediments. Ph.D. thesis, University of Kiel.

Orson, R., W. Panageotou, and S.P. Leatherman. 1985. Response of tidal salt marshes of the U.S. Atlantic and Gulf Coasts to rising sea levels. *Journal of Coastal Research* 1: 29–37.

Pedersen, J.B.T., and J. Bartholdy. 2007. Exposed salt marsh morphodynamics: An example from the Danish Wadden Sea. *Geomorphology* 90: 115–125.

Pedersen, J.B.T., J. Bartholdy, and C. Christiansen. 2007. 137Cs in the Danish Wadden Sea: Contrast between tidal flats and salt marshes. *Journal of Environmental Radioactivity* 97: 42–56.

Pethick, J.S. 1981. Long-term accretion rates on tidal salt marshes. *Journal of Sedimentary Research* 51: 571–577.

Redfield, A.C. 1972. Development of a New England salt marsh. *Ecological Monographs* 42: 201–237.

Reed, D.J. 1995. The response of coastal marshes to sea-level rise: Survival or submergence? *Earth Surface Processes and Landforms* 20: 39–48.

Reise, K., M. Baptist, P. Burbridge, N. Dankers, L. Fischer, B. Flemming, A.P. Oost, and C. Smit. 2010. *The Wadden Sea—a universally outstanding tidal wetland. Wadden Sea Ecosystem 29*, 7–24. Wilhelmshaven: Common Wadden Sea Secretariat.

Rockel, B., and K. Woth. 2007. Extremes of near-surface wind speed over Europe and their future changes as estimated from an ensemble of RCM simulations. *Climatic Change* 81: 267–280.

Temmerman, S., G. Govers, P. Meire, and S. Wartel. 2003a. Modelling long-term tidal marsh growth under changing tidal conditions and suspended sediment concentrations, Scheldt estuary, Belgium. *Marine Geology* 193: 151–169.

Temmerman, S., G. Govers, S. Wartel, and P. Meire. 2003b. Spatial and temporal factors controlling short-term sedimentation in a salt and freshwater tidal marsh, Scheldt estuary, Belgium, SW Netherlands. *Earth Surface Processes and Landforms* 28: 739–755.

The Trilateral Monitoring and Assessment Program—TMAP. 2006. Ubgkal07: Topographie DK und SH. Nationalpark Schleswig-Holsteinisches Wattenmeer. http://www.waddensea-secretariat.org/TMAP/Data-Unit/Data.html. Accessed 20 Nov 2008

van de Koppel, J., D. van der Wal, J.P. Bakker, and P.M.J. Herman. 2005. Self-organization and vegetation collapse in salt marsh ecosystems. *American Naturalist* 165: E1–E12.

von Storch, H., and R. Weisse. 2008. Regional storm climate and related marine hazards in the Northeast Atlantic. In *Climate extremes and society*, ed. H.F. Diaz and R.J. Murnane, 54–73. Cambridge: Cambridge University Press.

Wahl, T., J. Jensen, and T. Frank. 2010. On analysing sea level rise in the German Bight since 1844. *Natural Hazards and Earth System Sciences* 10: 171–179.

Walling, D.E., A.L. Collins, and H.M. Sichingabula. 2003. Using unsupported lead-210 measurements to investigate soil erosion and sediment delivery in a small Zambian catchment. *Geomorphology* 52: 193–213.

Williams, H. 2003. Modeling shallow autocompaction in coastal marshes using cesium-137 fallout: Preliminary results from the Trinity River Estuary, Texas. *Journal of Coastal Research* 19: 180–188.

Winterwerp, J.C. 2002. On the flocculation and settling velocity of estuarine mud. *Continental Shelf Research* 22: 1339–1360.

Woth, K., R. Weisse, and H. von Storch. 2006. Climate change and North Sea storm surge extremes: An ensemble study of storm surge extremes expected in a changed climate projected by four different regional climate models. *Ocean Dynamics* 56: 3–15.

WSA—Wasser- und Schifffahrtsamt Tönning. 2007. Wasserstandsinformationen: Hörnum/Sylt. http://www.wsv.de/wsa-toe/service/wasserstandinfo/index.html. Accessed 27 Aug 2010.

AUTHOR QUERIES

AUTHOR PLEASE ANSWER ALL QUERIES.

Q1. The citation “Malvren Mastersizer 2000” (original) has been changed to “Malvern Instruments Ldt 2010”. Please check if appropriate.
Q2. “Wahl et al. 2011” was cited here but not found in the reference list. Please provide complete bibliographic information.
Q3. Figure 3 – contains cut off data. Please provide replacement otherwise, please advise if we can proceed with the figure/s as is.
Q4. Please check if Table 1 was captured and presented correctly.
Q5. “Wahl (2010)” here has been changed to “Wahl (2010, personal communication)”. Please check.
Q6. Hartwig (2010) was cited here but not found in the reference list. Please provide complete bibliographic information.
Q7. De Groot (2009) was not cited anywhere in the text. Please provide a citation. Alternatively, delete the item from the list.
Q8. Kindly check if the provided publisher name here is correct.
Q9. Kirwan et al. (2010) was not cited anywhere in the text. Please provide a citation. Alternatively, delete the item from the list.